Digest Journal of Nanomaterials and Biostructures Vol. 9, No. 2, April - June 2014, p. 531 - 541

SYNTHESIS AND CHARACTERIZATION OF POLY (SODIUM 2-ACRYLAMIDO-2-METHYL PROPANE SULFONATE) / CLAY NANOCOMPOSIT ON STEEL IN AGGRESSIVE MEDIUM

A. M. ATTA[a,b*], G. A. EL-MAHDY[a,c], H. A. AL-LOHEDAN[a],
A. M. TAWFEEK[d], AHMED A. ABDEL-KHALEK[e]
[a]*Department of Chemistry, Surfactant Research Chair, College of Science, King Saud University, Riyadh 11451, Saudi Arabia*
[b]*Petroleum application department, Egyptian petroleum research institute, Nasr city 11727, Cairo, Egypt.*
[c]*Chemistry department, Faculty of Science, Helwan University, Helwan 11795, Egypt*
[d]*College of Science, King Saud University, Riyadh, Saudi Arabia.*
[e]*Chemistry department, Faculty of Science, Beni Suef University, Beni Suef, Egypt.*

Waterborne bioactive materials PNa- AMPS /MMT has been successfully prepared by effectively dispersing inorganic nanolayers of Na+-MMT clay in crosslinked PNa- AMPS matrix through direct aqueous solution dispersion technique. The prepared nanogel was characterized by Fourier transform infrared (FTIR), X-ray diffraction (XRD) patterns and transmission electron microscopy (TEM). The corrosion inhibition activity of PNa-AMPS /MMT towards steel corrosion in chloride containing environment has been investigated by polarization and electrochemical impedance spectroscopy (EIS) methods. Polarization measurements indicate that PNa-AMPS /MMT acts as a mixed type-inhibitor and the inhibition efficiency increases with inhibitor concentration. The results of potentiodynamic polarization and EIS measurements clearly showed that the inhibition mechanism involves blocking of the steel surface by inhibitor molecules via adsorption.

(Received January 30, 2014; Accepted April 11, 2014)

Keywords: Nanoclay; nanogel; Sodium 2-acrylamido-2-methylpropane sulfonate; Nanocomposite

1. Introduction

Clay particles have been employed as encapsulating components within a polymer matrix to enhance cell growth and as additives in dental adhesives to improve shear bond strength, to tailor the tensile/mechanical properties or to affect in vitro degradation rates [1–5]. In addition, Clays have various industrial applications in plastic materials for food packaging and as rheological modifiers for paints, inks, and greases due to its intercalating properties, availability, and relatively low cost materials [6-7]. In the last decades, among the various available nanoparticles, nanoclay and its derivatives are widely used clay nanocomposites as anticorrosion in the form of organic coatings [8-14]. The unique properties, together with relatively low material cost, provide a great attraction in polymer science and technology toward the commercialization of the clay-based nanocomposites. The polymeric organic coatings are usually used to protect metals against corrosion and this is most likely achieved by means of barrier properties against water, oxygen or/and corrosive ions such as; Cl^- and H^+. Moreover, it was found that the incorporation of organoclay into polymer composites may effectively enhance the anticorrosion effect of as-prepared polymeric coatings [11,-12]. Smaller inorganic filler particles may increase polymer–filler interactions and also improve barrier properties of the host polymeric coating. Hence, highly dispersed nano-sized particles provide enhanced barrier properties in comparison with

* Corresponding author: aatta@ksu.edu.sa

conventional fillers [14]. The inclusion of clay nanoparticles into polymer composites can improve the corrosion resistance of the coating film via enhancing barrier properties. The extent of the improvement; however, greatly depends on the nanoparticles content and the clay dispersion and, the best results are reported with the exfoliated systems [15].

Recently, the preparation of polymer–clay nanocomposite materials has directed to develop new water-based system. Currently, smectite clays (e.g., montmorillonite, MMT) is a popular layered material for the preparation of polymer–clay nanocomposites, because of they offer large surface area. It was reported that, the hydrophilic (MMT) clay shows better dispersion capability than organo-clay which leads to a much enhanced anticorrosion performance on metallic surface [16]. The clay nanocomposite materials can be prepared through in situ emulsion polymerization (i.e., water-based latex) [17–21], and suspension polymerization [17, 19]. Several works have usually adopted certain organic modifications for clay to access exfoliated polymer–clay nanocomposites [22–26]. To the best of our knowledge up to date, few processes have been employed without the pretreatment of the clay. In this respect, the sadium-2-acrylamido-2-methylpropane sulfonate (Na-AMPS) monomer is found to be highly soluble in water, and MMT is also hydrophilic in nature. It is possible to prepare exfoliated nanocomposites through aqueous polymerization which has the advantage that all the ingredients are added to a single reactor, avoiding the two steps that are necessary when using an in situ polymerization technique: clay treatment and then a separate polymerization after dispersing that treated clay in the monomer. In our previous works [27-31], we reported that the nanogel composites containing nano-metals such as silver and magnetite have strong ability to protect steel materials with low concentrations more efficiently than that of the conventional organic inhibitors. The data indicated that the nanogel particles have the advantages over normal organic inhibitors due to the formation of uniform thin film on the surface of steel, which entirely cover all surface without any defects. The data claimed the exceptional improvement in performances for these inhibitors are associated with increasing of barrier properties, prevention of charge transportation by the nanosize, as well as very large surface area availability for the liberation of dopant due to the presence of nanosize materials. Recently Chang et al. [32] found that introduction of MMT into organic coatings may increase the length of diffusion pathways for oxygen and water as well as decreasing permeability of the coating which are reflecting a significant enhancement in corrosion protection on metallic surface. In the present work, it should be valuable to explore the application of clay coated poly (sodium 2-acrylamido-2-methyl propane sulfonate) nanocomposite (PNa- AMPS /MMT) as corrosion inhibitors for steel in aggressive acidic medium. The prepared composites will be evaluated as an effective anticorrosion behavior of a hydrophobic surface on stainless steel. The inhibition effect of PNa- AMPS /MMT composites on steel corrosion in 1M HCl solution was investigated using potentiodynamic polarization curves and electrochemical impedance spectroscopy (EIS).

2. Experimental

2.1 Materials

Nanoclay (sodium montmorillinite; Na^+ MMT) hydrophilic was purchased from Sigma-Aldrich Co. (St. Louis, MO, USA) with commercial name `Nanomer ® PGV. Sodium 2-acrylamido-2-methylpropane sulfonate (Na AMPS), poly(vinyl pyrrolidone) (PVP) with molecular weight 40,000 g/mol, *N,N*-methylene bisacrylamide (MBA), ammonium persulfate (APS), and *N*,*N*,*N*′,*N*′-tetramethylethylenediamine (TEMED) were obtained from Sigma Chemicals (St Louis, MO, USA). All reagents were used as received, and double deionized (DDI) water prepared with a UVO ultrapurification system (Millipore, Billerica, MA, USA) was used throughout the work.

2.2 Method of preparation:

The nanogel latex was synthesized using free radical copolymerization of Na-AMPS in the presence of MBA as a crosslinker. Atypical preparation procedure of nanogel is described as follows: In one 100 mL round-bottom flask, 0.125 g of Na-MMT and 0.5 g PVP were mixed with

50 mL of EtOH/H_2O (2/1 volume ratio). The solution was stirred at room temperature for 2 h. The flask was purged with nitrogen, and the monomers, a mixture of Na-AMPS (1.2 g) and 28.3 µl of MBA were successively introduced at room temperature under stirring. Finally, 0.0125 g KPS initiator (dissolved in 3ml H_2O) and 20 µl TEMED were added to the system under continuous stirring at an ice–water temperature. The polymerization was allowed to proceed at 20 °C for 24 h. The produced polymer separated after ultracentrifuge at 21000 rpm for 30 minute and designated as PNa-AMPS /MMT.

2.3 Characterization

Fourier Transform infrared (FTIR) spectroscopic analysis of the samples was performed using a Spectrum One FTIR spectrometer (Perkin-Bhaskar-Elmer Co., Boston, MA, USA). The morphology and structure of the prepared magnetic nanoparticles were determined using high-resolution transmission electron microscopy (HR-TEM). HR-TEM images of the nanocomposites were recorded using a JEM-2100 F (JEOL, Tokyo, Japan) at an acceleration voltage of 150 kV. The particle size distributions (PSDs) were determined from TEM microphotographs on representative samples of more than 1,000 particles of magnetic latexes and analyzed using the Bolero software (AQ Systems, Sweden).

XRD analysis of the MMT and nanogel was performed using an X-ray diffractometer (X'Pert, Philips, Netherlands) with Cu Kα radiation of wavelength 1.54 Å, operating at a voltage of 40 kV and a current of 40 mA at a rate of 2° min^{-1} and in the range $2\theta = 0–10^\circ$.

2.4. Electrochemical Measurements

The steel compositions were checked by Optical Emission Spectroscopy which showed following (wt%): 0.14% C, 0.57% Mn, 0.21% P, 0.15% S, 0.37% Si, 0.06% V, 0.03% Ni, 0.03% Cr and Fe (balance). The steel specimens for corrosion tests were finished by grinding with 4000-grit silicon carbide paper. The electrochemical tests were conducted using a Solartron 1470E system (multichannel potentiostat) with Solartron 1455A as frequency as frequency response analyzer for AC measurements. The peak to peak amplitude of the sinusoidal perturbation was 10 mV. The frequency ranged from 10 kHz to 10 mHz. Electrochemical experiments were carried out in a Pyrex cell with three compartments. A platinium counter electrode (CE) was used with a saturated calomel electrode (SCE) as reference electrode (RE). Data were collected and analysed using CorrView, Corr- Ware, Zplot and ZView software.

3. Results and discussion

The majority of the literature associated with the studies of polymer–clay nanocomposite materials published in past decade are mainly organic solvent-based. However, the research interests have shifted recently to the studies of water-based systems due to the increasing environmental and health issues. Encapsulation of MMT by PNa-AMPS has been achieved using dispersion polymerization, with the aid of PVP as stabilizer. To prepare a of PNa-AMPS/clay, in this study, suitable amount of raw hydrophilic Na+- MMT clay was effectively dispersing in as-prepared Na-AMPS, by solution dispersion technique under vigorously magnetically stirring. The composition of the PNa-AMPS/clay materials was varied from 0 to 3 wt% of Na+-MMT clay with respect to the PNa-AMPS. On the other hand, H_2O/EtOH solvent system is used to obtain high dispersion MMT nanoparticles. Ethanol/water mixture acts as non-solvent for PNa-AMPS, so PVP is used as a polymeric stabilizer to achieve excellent colloidal stability of core shell nanoparticles. Too low concentration may be insufficient to stabilize all nanoparticles leading to particles coalescence. Excess stabilizer at any stage of polymerization may cause further nucleation to occur. Monomers and PVP must be stirred vigorously for a long time before starting the polymerization reaction to ensure insertion of Na-AMPS monomer between the clay galleries. The concentration of monomers affects the morphology of nanocomposite. Too low concentration of monomers leads to irregular morphology, while high concentration increases the particle size

and leads to aggregations. High concentration of clay failed to give stable colloidal core shell nanogel and aggregation of clay occur prior to polymerization. The stages of the preparation of crosslinked PNa-AMPS/clay was illustrated in the **Scheme 1**. Stage (a) represents the intercalation to prepare MMT and stage (b) represents the crosslinking polymerization of monomer Na-AMPS in the presence of purified MMT and water-soluble crosslinker MBA.

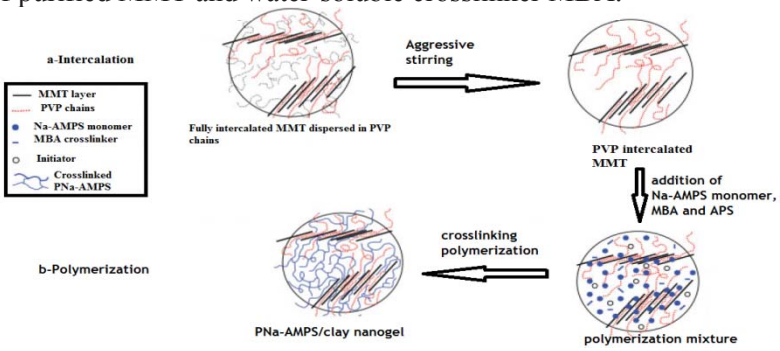

Scheme 1: Preparation of PNa-AMPS/clay nanogel.

3.1 Chemical Structure of PNa-AMPS/clay nanogel:

The representative FTIR absorption spectra of the intercalated Na^{+}MMT /PVP, PNa-AMPS/clay nanogel were given in Figure 1. The characteristic vibration bands of Na+-MMT clay were shown at bands at 465 and 527 cm-1 are corresponded to Si-O-Si and Al-O-Si bending vibrations. The band at 634 cm-1 is assigned to the out-of-plane vibrations of coupled Al-O and Si-O.

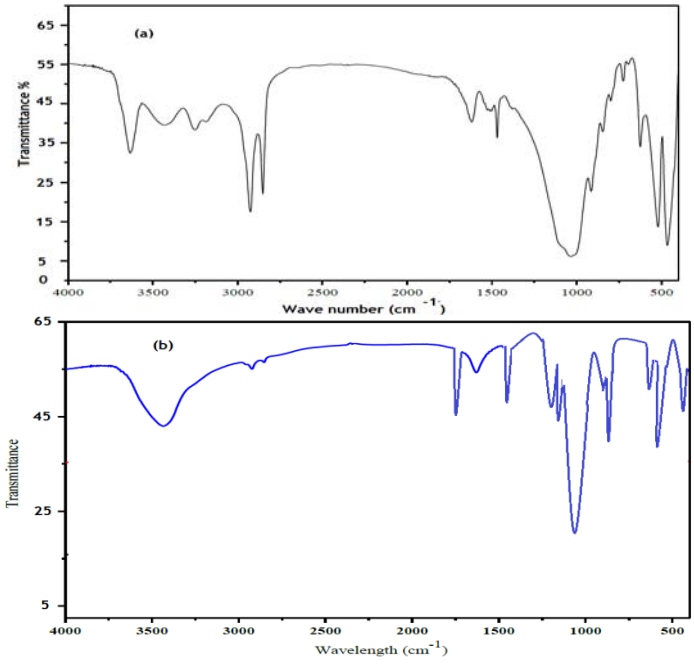

Fig. 1. FTIR specta of a) Na^{+}-MMT and b) PNa-AMPS/clay nanogel.

The band at 848 cm-1 is assigned to the bending vibration of Al-Mg-OH. The spectral band at 919 cm-1 reflects the stretching vibration of Al-O-(OH)-Al, 1040 (Si–O), 600 (Al–O) and 420 cm^{-1} (Mg–O) [33, 34]. The strong band at 1040 cm^{-1} represents the Si-O-Si groups of the tetrahedral sheet. The spectral band at 1648 cm^{-1} reflects the bending of CON- bond of PVP, which is retained in the matrix. The peaks at 2854 and 2925 cm^{-1} are assigned to the aliphatic C-H stretching vibration of the methylene and methyl group CH2 of the aliphatic chain of PVP. Also, C-H in plane bending vibration of the methylene groups can be seen at wavelength bands of 1477

cm^{-1}, verifying the intercalation of PVP molecules between the silica layers. The broad band at 3436 cm^{-1} is due to H-OH stretching vibration of the water molecules adsorbed on the solid surface. The strong band at 3637 cm-1 attributed to O-H stretching vibration of the silanol (Si-OH) groups from the solid (OH groups between octahedral and tetrahedral sheets) and Al(Mg)–O–H stretching vibration. The FTIR spectrum of PNa-AMPS/clay nanogel nanogels incorporated with 10 wt% clay represented in Figure 1b. The absorption bands in the range of 3400– 3700 cm^{-1} are attributed to the stretching of –OH of clay and NH of MBA and Na-AMPS. The absorption bands at 1090 cm^{-1} and 1643 cm^{-1} attributed to SO and CONH stretching of Na-AMPS, respectively. After incorporated into the PNa-AMPS polymeric network, the –OH stretching of various clays in the range of 3400–3700 cm^{-1} disappeared and the absorption bands at about 1030 cm^{-1} ascribed to Si–O stretching of clays were weakened as shown in Figure 1 b. The disappeared

and weakened absorption bands may be according to the interaction between clays with Na-AMPS during the polymerization process**[35]**. The bands at 1364 and 1241 cm^{-1} (S=O), NH bending 1543 cm^{-1} are related to Na-AMPS.

3.2 XRD analysis of PNa-AMPS/clay nanogel

The chemical structures of hydrophilic Na^{+}-montmorillonite (Na+-MMT) clay used consisting of two fused silica tetrahedral sheets sandwiching an edge-shared octahedral sheet of either magnesium or aluminum hydroxide and small cations such as sodium or potassium located in silicate interlayer galleries, providing an opportunity for cationic exchange reactions between the small cations and larger cationic surfactant molecules to render the hydrophilic layered silicate organophilic. XRD technique was used for the characterization of clay-filled nanocomposites. This technique allows determining the spaces between the silicate layers by using Bragg's formula $n\lambda=2d \sin\theta$, where λ represents wavelength of X-ray radiation used in the diffraction experiment, d is the distance between diffraction lattice planes and θ stands for the diffraction angle or glancing. The XRD of MMT and PNa-AMPS/clay nanogel were represented in Fig. 2.

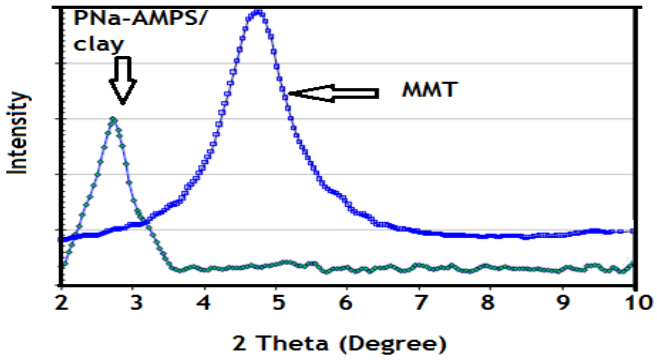

Fig. 2. XRD pattern of MMT and PNa-AMPS/clay nanogel.

The peak appeared at 6.7–7.0° shown in Figure 2 corresponds to the periodicity in the (001) direction of Na+-MMT clay. The data indicated that PNa-AMPS/clay nanogel shows peak at $2\theta = 2.74^{o}$ (d spacing = 14.27 nm) while MMT clay has peak at $2\theta = 4.86^{o}$ (d spacing = 12.29 nm). These data are suggesting the possibility of having exfoliated silicate layers of hydrophilic MMT dispersed in PNa-AMPS matrix [**36**]. It is believed that the increase in d-spacing of the silicate layers happens via both shear and diffusion mechanisms [37].

3.3 Morphology of PNa-AMPS/clay nanogel:

The morphological image studies for dispersion capability of Na+-MMT and MMT-PVP clay in PNa-AMPS matrix can be further compared and evidenced by the observation of transmission electron microscopy (TEM), as shown in Figure 3. The nanoclay changed from

laminar to spherical core-shell when treated with PVP as illustrated in Figure 3 a and b, respectively. The size (diameter) of spherical and the thickness (height) of laminar particles are in nanoscale. TEM provide the best proof for success encapsulation of MMT-PVP within PNa-AMPS matrix as represented in Fig. 3 c. The image reveals that core shell structure with will defined morphology is successfully prepared. The PNa-AMPS completely surround the MMT-PVP, the particle size was ranged from 21 to 38 nm.

(a)

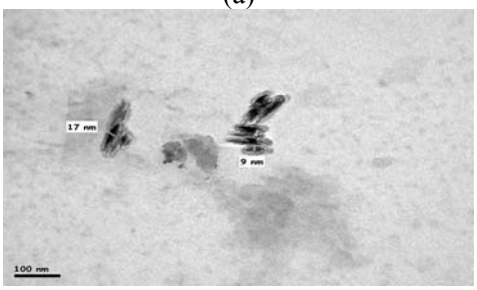

(b)

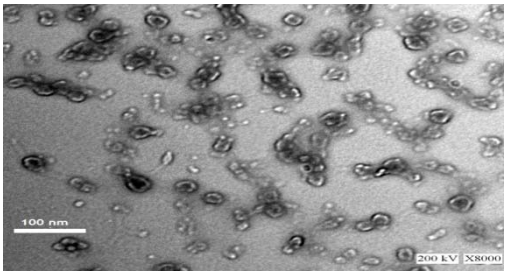

(c)

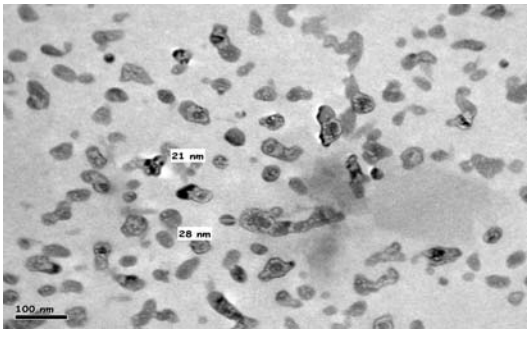

Fig. 3: TEM micrographs of a) Na-MMT, b) Na-MMT/PVP and c) PNa-AMPS/clay nanogel.

It is highly probable that the mechanism of polymerization plays an important role in the final particle sizes and morphology. Indeed, in conventional dispersion polymerization, the particle size is dependent on the solubility of the polymer in the dispersion medium and on the amount or nature of the stabilizer [**38**]. An excess of stabilizer at any stage of the polymerization can cause further nucleation to occur, while a deficiency of stabilizer leads to particle coalescence. From the dispersant-limited agglomeration theory [**39**], it is known that the polymer particles result from the agglomeration of much smaller primary particles that are initially unstable. The stabilizer, which is insufficient to cover the total surface area of the primary particles, redistributes onto the reduced

surface area of the aggregates and prevents further agglomeration. In our case, this process could occur with the small clay particles. Indeed, the polymer at the clay surface offers a surface area with the continuous phase that increases when the clay patrticle size decreases. Therefore, as the size of the clay nanopatrticle decreases, associations between composite particles could happen until the concentration of stabilizer at the surface of the polymer is high enough to ensure a good stabilization of the particles which then contain several clay particles. The TEM images of both MMT-PVP within PNa-AMPS exhibited mainly exfoliated structures. This conclusion implied that Na+-MMT clay platelets showing a better dispersion capability in PNa-AMPS matrix, which is consistent with the previous XRD studies. From the above analysis, a structural model of nanogel system including clay could be derived. This structural model indicates clay layers inside the nanocomposite. The exfoliated single platelets randomly dispersed in the PNa-AMPS matrix and paying attention to the model it is found that there is a difficult and unintelligible path toward steel substructure for H_2O molecules.

3.4 potentiodynamic polarization measurements

Fig. 4 shows the potentiodynamic polarization curves of steel without and with PNa-AMPS /MMT clay addition in 1 M HCl solution. The addition of PNa- AMPS /MMT clay significantly reduced the anodic and cathodic current density indicating the mixed mode of inhibition. In other words, both cathodic and anodic reactions of steel electrode are retarded by the addition of clay in hydrochloric acid solution. The results can be explained on the basis that the anodic process occurring on the electrode substrate was obstructed as well as a reduction of cathodic reaction. This can be attributed to the formation of a protective film on steel surface [**40-42**].

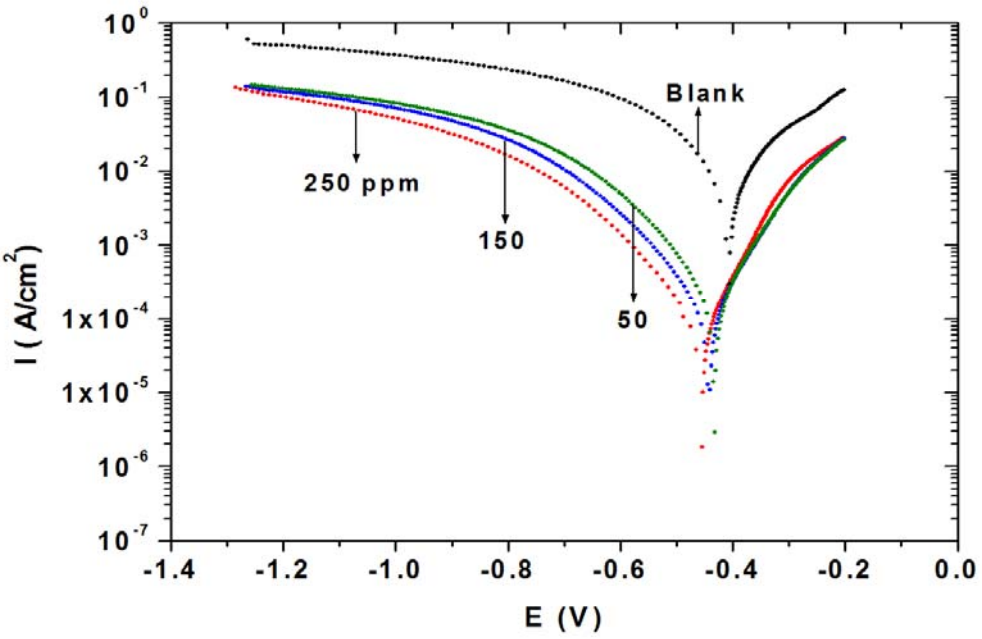

Fig.4. Potentiodynamic polarization curves of steel immersed in 1M HCl solution containing different PNa- AMPS /MMT clay concentrations.

The electrochemical corrosion parameters of corrosion as current densities (i_{corr}), corrosion potential (Ecorr), cathodic Tafel slope (Bc), and anodic Tafel slope (Ba) as functions of inhibitor concentration are given in Table1. Apparently, Icorr decreases prominently with the inhibitor concentration. The inhibition efficiencies were obtained by the following relationship [43-44]:

$$IE(\%) = 1 - i_{corr\,(2)} / i^{o}_{corr\,(1)} \quad (1)$$

where $i^{o}_{corr(1)}$ and $i_{corr(2)}$ are the uninhibited and the inhibited corrosion current densities, respectively. The values of IE% were calculated and listed in Table 1. The observed increase in IE% with increasing PNa- AMPS /MMT clay concentration can be attributed to an increase in the surface coverage. The results can be explained on the basis that that the inhibitor molecules might be adsorb on the steel surface and cover active sites of the electrode surface, thereby protecting these sites from attack by chloride ions resulting in high corrosion performance of the inhibitor.

Table 1: Inhibition efficiency values for steel in 1M HCl with different concentrations of PNa- AMPS /MMT clay calculated by polarization and EIS methods.

	Polarization Method					EIS Method		
	B_a (mV)	B_c (mV)	E_{corr} (V)	i_{corr} μA/cm^2	IE%	R_{ct} Ohm	C_{dl} (μF/cm^2)	IE%
Blank	147.00	141.00	-0.4034	745	_____	1.80	334	____
50 ppm	93.68	111.91	-0.4323	192.82	74.11	7.58	184	76.25
150	88.60	115.02	-0.4418	128.53	82.747	14.6	139	87.67
250	77.41	112.68	-0.4553	80.58	89.18	19.3	116	90.67

3.5 EIS measurements

Nyquist plots for the corrosion of steel in 1.0 M HCl solution in the presence of different concentrations of PNa- AMPS /MMT clay are shown in Fig. 5. It can be observed from the figure that the diameter of the semicircle increases with the increase in the concentration of clay, indicating that the corrosion of steel is mainly controlled by a charge transfer process [**45**]. In addition, the diameter of the capacitive loop in the presence of inhibitor is larger than that in the absence of inhibitor (blank solution), and increases with the inhibitor concentration.

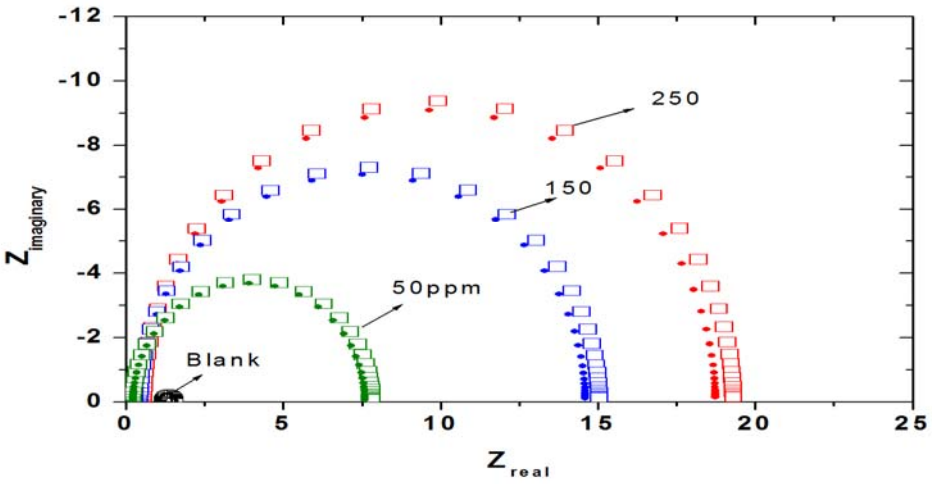

Fig. 5. Nyquist plots of steel immersed in 1M HCl solution containing different PNa- AMPS /MMT clay concentrations

The impedance data were analyzed using an equivalent circuit shown in Figure 3, which enables the calculation of numerical values corresponding to the physical and/or chemical properties of the electrochemical system under investigation [46]. The circuit consists of the electrolyte solution resistance (Rs), charge transfer resistance (Rct) double layer capacitance (Cdl). The values of Rct and Cdl were determined and listed in Table 1.

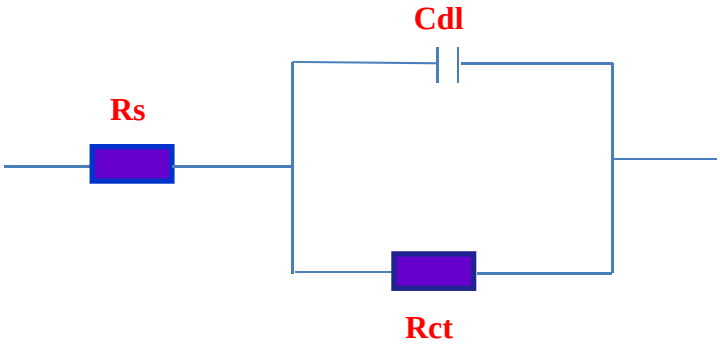

Fig.6. Equivalent circuit employed in fitting EIS data

Clearly, Rct increases prominently, while Cdl reduces with the concentration of clay. A better protection provided by an inhibitor is accompanied by lowering values of Rct, which can be associated with a slower rate of corrosion and a decreasing in the values of double layer capacitance of the steel. The values of Rct increase with the increase in the concentration of clay, suggesting that the amount of the inhibitor molecules adsorbed on the electrode surface increases as the concentration of PNa- AMPS /MMT clay increases. The decrease in Cdl in comparing with that in blank solution (without inhibitor), can be attributed to a decrease in local dielectric constant and/or an increase in the thickness of the electrical double layer. The inhibition efficiencies were calculated and listed in Table 1 using the following equation:

$$IE\% = 1- Rct_{(1)}/R^2ct_{(2)} \times 100 \quad (2)$$

where $R_{ct(1)}$ and $R_{ct(2)}$ are the charge transfer resistances in absence and presence of the inhibitors, respectively. As can be seen from Table 1, the inhibition efficiencies increase markedly with increasing clay concentration. The EIS data suggests that a barrier protective film forms on the surface and therefore, a higher degree of inhibition was obtained with increasing clay addition to 1 M HCl solution. Inhibition efficiencies obtained from potentiodynamic polarization curves and EIS are in good reasonably agreement.

4. Conclusions

The following conclusions can be withdrawn from the above results:

- Exfoliated hydrophilic clay was prepared after treatment of the hydrophilic clay with PVP in aqueous ethanolic solutions.
- TEM indicated the conversion of hydrophilic clay laminar to spherical core-shell when treated with PVP.
- The data indicated the MMT clay was encapsulated in PNa-AMPS Matrix.
- PNa- AMPS /MMT clay acts as a mixed-type inhibitor in 1.0 M HCl.
- The results obtained from EIS and polarization studies are in a good agreement for increasing the inhibition efficiency values with PNa- AMPS /MMT clay concentration

Acknowledgment

The authors extend their appreciation to the Deanship of Scientific Research at King Saud University for funding the work through the research group Project No. RGP-VPP-148.

References

[1] H. A. Patel, R. S. Somani, H. C. Bajaj, RV Jasra. Bull Mater Sci **29**, 133 (2006).
[2] Pereira de Abreu DA, Paseiro Losada P, Angulo I, Cruz JM. Eur Polymer J **43**, 2229 (2007).
[3] Atai M, Solhi L, Nodehi A, Mirabedini SM, Kasraei S, Akbari K, Dental Materials **25**, 339 (2009).
[4] K. F. Lin, CY Hsu, TS Huang, WY Chiu, YH Lee, TH Young. J Appl Polym Sci **98**, 2042 (2005).
[5] H. Zhuang, J.P. Zheng, H Gao, KD Yao. J Mater. Sci. Mater. Med. **18,** 951 (2007).
[6] Styan KE, Martin DJ, Poole-Warren LA. J Biomed Mater Res Part A **86A(3),** 571 (2007);.
[7] H.M. Lewkowitz-Shpuntoff, MC Wen, A Singh, N Brenner, R Gambino, N Pernodet, Biomaterials **30**, 8 (2009).
[8] J-M. Yeh, T-H. Kuo, H-J. Huang, K-C. Chang,M-Y. Chang, J-C. Yang, European Polymer Journal **43**, 1624 (2007).
[9] K-C. Chang, S-T. Chen, H-F. Lin, C-Y. Lin, H-H. Huang, J-M. Yeh, Y-H. Yu, European Polymer Journal **44**, 13–23 (2008).
[10] M. Behzadnasab, S.M. Mirabedini, M. Esfandeh, Corrosion Science **75**, 134(2013).
[11] J.M. Yeh, C.L. Chen, Y.C. Chen, C.Y. Ma, K.R. Lee, Y. Wei, S. Li, Polymer **43**, 2729 (2002).
[12] J.M. Yeh, C.P.Chin, J Appl Polym Sci **88**,1072 (2003).
[13] S. Sinha Ray, M. Okamoto, Prog. Polym. Sci. **28**, 1539(2003).
[14] V. Saji, J. Thomas, Nanomaterials for corrosion control, Curr. Sci. **92**, 51 (2007).
[15] C. Chen, M. Khobaib, D. Curliss, Prog.Org. Coat. **47**, 376 (2003).
[16] K-C. Chang, M-C. Lai, C-W. Peng, Y-T. Chen, J.M. Yeh, C-L. Lin, JC.Yang, Electrochim Acta **51**, 5645 (2006).
[17] X. Huang, W.J. Brittain, Macromolecules **34**, 3255 (2001).
[18] P. Meneghetti, S. Qutubuddin, Langmuir **20**, 3424 (2004).
[19] D. Wang, J. Zhu, Q. Yao, C.A.Wilkie, Chem. Mater. **14**, 3837 (2002).
[20] D.C. Lee, L.W. Jang, J Appl Polym Sci **61**, 1117 (1996).
[21] Y.S. Choi, M.H. Choi, K.H. Wang, S.O. Kin, Y.K. Kim, I.J. Chung, Macromolecules **34**, 8978 (2001).
[22] X. Hu, J.R. Meng, J. Polym. Sci. Part A Polym. Chem. **43**, 994 (2005).
[23] M.W. Weimer, H. Chen, E.P. Giannelis, D.Y.Sogah, J. Am. Chem. Soc. **121**, 1615 (1999).
[24] X. Fan, C. Xia, R.C.Advincula, Langmuir **21**, 2537 (2005).
[25] Y.S. Choi, I.J. Chung, Polymer **45**, 3827 (2004).
[26] X. Huang, W.J. Brittain, Macromolecules **34**, 3255 (2001).
[27] A.M. Atta, O.E. El-Azabawy, H.S. Ismail, M.A. Hegazy, Corros. Sci. **53**, 1680–1689 (2011).
[28] G. A. EL-Mahdy, A.M. Atta, A.K. F. Dyab, H.A. Allohedan, J.Chemistry, Article ID 125731. doi.org/10.1155/2013/125731 (2013).
[29] A. M. Atta, G. A. El-Mahdy, H. A. Al-Lohedan, Int. J. Electrochem. Sci., **8**, 4873 (2013).
[30] A.M. Atta, H.A. Allohedan, G.A. El-Mahdy, A-R. O. Ezzat, Journal of Nanomaterials, Article ID 580607, 8 pages http://dx.doi.org/10.1155/2013/580607 (2013).
[31] G. A. El-Mahdy, A.M. Atta, H. A. Al-Lohedan, *Molecules, in Press 19* (**2014).**
[32] K.C. Chang, G.W. Jang, C.W. Peng, C.Y. Lin, J.C. Shieh, J.M. Yeh, J.C. Yang, W.T. Li, Electrochim. Acta **52**, 5191–5200 (2007).
[33] F.Q. Zhang, Z.J. Guo, H. Gao, Y.C. Li, L. Ren, L. Shi, L.X. Wang, Polym. Bull. **55**, 419 (2005).
[34] A. Li, A. Wang, J. Chen, J. Appl. Polym. Sci., **92**, 1596-1603 (2004).

[35] J. Zhang, A. Wang, Reactive & Functional Polymers **67**, 737–745 (2007).
[36] J-M. Yeh, C-T. Yao, C-F. Hsieh, L-H. Lin, P-L. Chen, J-C. Wuc, H-C. Yang, C-P. Wua, Eur. Polym. J. **44**, 3046–3056(2008).
[37] S.S. Ray, M. Okamoto, Prog. Polym. Sci. **28**, 1539 (2003).
[38] A.J. Paine, Macromolecules, **23**, 3109 (1990).
[39] N.D. Nam, J.G. Kim, S.M. Park, N.E. Lee, , Met. Mater. Int. **14**, 197 (2008).
[40] N.D. Nam, J.H. Ahn, N.E. Lee, J.G. Kim, Mater. Res. Bull. **45**, 269 (2010).
[41] A. Lalitha, S. Ramesh, S. Rajeswari, Electrochim. Acta **51**, 47 (2005).
[42] H. Shokry, M. Yuasa, I. Sekine, R.M. Issa, H.Y. El-Baradie, G.K. Gomma, Corros. Sci. **40**, 2173 (1999).
[43] S. Li, S. Chen, S. Lei, H. Ma, R. Yu, D. Liu, Corros. Sci. **41**, 1273 (1999).
[44] S. Li, Y.G. Wang, S. Chen, R. Yu, S. Lei, H. Ma, D. Liu, Corros. Sci. **41,** 1769(1999).
[45] M. Behpour, S.M. Ghoreishi, N. Mohammadi, N. Soltani, M. Salavati-Niasari, Corros. Sci. **52**, 4046 (2010).
[46] A.R.S. Priya, V.S. Muralidharam, A. Subramania, , Corrosion **64,** 541 (2008).